JACS
JOURNAL OF THE AMERICAN CHEMICAL SOCIETY
Article
pubs.acs.org/JACS

Efficient Visible Light Nitrogen Fixation with BiOBr Nanosheets of Oxygen Vacancies on the Exposed {001} Facets

Hao Li, Jian Shang, Zhihui Ai, and Lizhi Zhang*

Key Laboratory of Pesticide & Chemical Biology of Ministry of Education, Institute of Environmental Chemistry, College of Chemistry, Central China Normal University, Wuhan 430079, PR China

Supporting Information

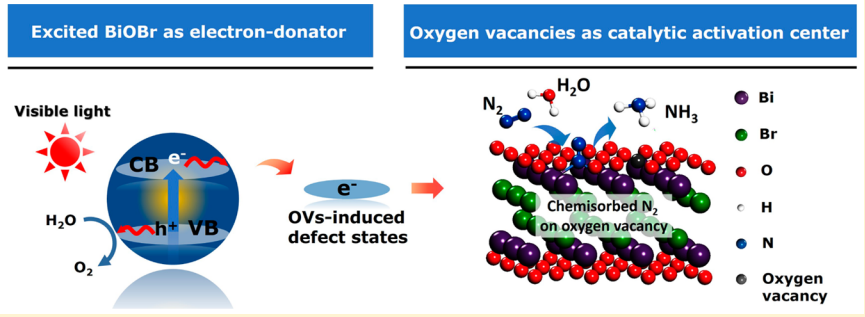

ABSTRACT: Even though the well-established Haber−Bosch process has been the major artificial way to "fertilize" the earth, its energy-intensive nature has been motivating people to learn from nitrogenase, which can fix atmospheric N_2 to NH_3 in vivo under mild conditions with its precisely arranged proteins. Here we demonstrate that efficient fixation of N_2 to NH_3 can proceed under room temperature and atmospheric pressure in water using visible light illuminated BiOBr nanosheets of oxygen vacancies in the absence of any organic scavengers and precious-metal cocatalysts. The designed catalytic oxygen vacancies of BiOBr nanosheets on the exposed {001} facets, with the availability of localized electrons for π-back-donation, have the ability to activate the adsorbed N_2, which can thus be efficiently reduced to NH_3 by the interfacial electrons transferred from the excited BiOBr nanosheets. This study might open up a new vista to fix atmospheric N_2 to NH_3 through the less energy-demanding photochemical process.

INTRODUCTION

Nitrogen is needed by all living organisms to build proteins, nuclei acids and many other biomolecules. Though constituting about 78% of the Earth's atmosphere, nitrogen, in its molecular form, is unusable to most organisms because of its strong nonpolar N−N covalent triple bond toward dissociation, negative electron affinity, high ionization energy and so on.[1] Thus, the industrial fixation of N_2 to NH_3 through the classical Haber−Bosch process has to be conducted under drastic conditions (15−25 MPa, 300−550 °C) in the presence of iron-based catalyst to overcome the kinetic limitation, while consuming 1−2% of the world's annual energy supply and producing 2.3 tons of fossil-derived CO_2 per year.[2,3] So far, the hydrogen gas used for the NH_3 synthesis is primarily generated from the steam reforming of methane, which uses up to 3−5% of the world's annual natural gas production and releases large quantities of CO_2.[4] In view of the fossil fuels shortage and global climate change, nitrogen fixation through less energy-demanding process is therefore a challenging and long-term goal.

In contrast, nature uses nitrogenase in vivo to catalytically reduce N_2 to NH_3 under mild conditions, accounting for over 60% of the total atmospheric N_2 fixed in the biogeochemical nitrogen cycle.[5] The most abundant and best characterized nitrogenase is the Mo-dependent enzyme composed of two indispensable metalloproteins working in tandem, which are respectively the electron-donating iron (Fe-) protein and the catalytic molybdenum−iron (MoFe-) protein.[6,7] At the core of MoFe-protein lies the important metal cluster of MoFe-cofactor, where N_2 is reduced by electrons provided by Fe-protein to yield NH_3. The binding and activation of N_2 on the MoFe-cofactor theoretically and experimentally explain why the entire biological N_2 fixation process is less "up-hill".[8,9] Although the exact mechanism is still unknown, concerted nature of the biological N_2 fixation process has inspired us that efficient N_2 fixation under mild conditions may be feasible if both the electron-donator and the catalytic activation center are presented and can well collaborate with each other.

Among many pioneering work to duplicate the reactions of nitrogenase, the heterogeneous photocatalytic strategy with the features of plant photosynthesis is very promising for the sustainable development. This is because the photocatalytic strategy employs inexpensive semiconductors as the catalysts, water as the solvent, and solar energy as the driving force, while the use of any costly organic solvents, reducing agents and

Received: March 25, 2015
Published: April 15, 2015

DOI: 10.1021/jacs.5b03105
J. Am. Chem. Soc. 2015, 137, 6393−6399

strong acids as well as the input of thermal/electric energy are no longer required.[10] Unfortunately, the efficiency of the state-of-the-art semiconductor photocatalytic N_2 fixation is far from satisfactory due to the poor interfacial charge transfer,[11−13] as most photoexcited electrons tend to recombine with their twinborn holes, rather than to be captured by the adsorbed N_2. Moreover, in comparison with the photocatalytic H_2 evolution and CO_2 reduction, photocatalytic N_2 fixation is more challenging because the N_2 fixation is seriously hampered by the high-energy N_2 intermediates in the reduced or protonated form (N_2^- or N_2H).[14] For example, the reduction potential of the N_2^- formation is as negative as −4.2 V vs NHE via $N_2 + e^- \rightarrow N_2^-{}_{(aq)}$. Though the proton-coupled electron transfer ($N_2 + H^+ + e^- \rightarrow N_2H$), the reduction potential becomes less negative (−3.2 V vs NHE), which is still not energetically accessible for traditional semiconductors (TiO_2, ZnO, Fe_2O_3, and CdS) in the absence of any organic scavengers and precious-metal cocatalysts. Therefore, fabricating electron-donating semiconductors with well-designed catalytic activation center capable of activating the N−N triple bond as with the MoFe-cofactor of nitrogenase might offer an accessible kinetic pathway toward the efficient photocatalytic N_2 fixation.

To realize this goal, we propose the introduction of oxygen vacancies (OVs) on the semiconductors surface. First, OVs with abundant localized electrons are of particular interests for the enhanced adsorption and activation of inert gas molecules. For example, OVs of TiO_2 can directly activate O_2 to reactive oxygen species such as $\bullet O_2^-$, O_2^{2-} and O_4^{2-}, depending on its coverage and adsorption geometry,[15,16] while CO_2 can be indirectly activated to $\bullet CO_2^-$, which is the rate-limiting step for CO_2 reduction.[17,18] However, the feasibility of OVs for the N_2 activation remains unexplored. Second, surface OVs with their typical defect states can trap electrons or holes to inhibit the charge carriers' recombination, and may also promote the transfer of these trapped charge carriers to the adsorbates. Moreover, the transiently charged electronic states of adsorbates through in situ activation by transitional metals or OVs can remarkably lower the energy barrier for the interfacial charge transfer.[19−21] To confirm this opinion, visible-light-responsive BiOBr was selected as the model semiconductor because of its suitable energy band positions and layered structure (characterized by $[Bi_2O_2]$ slabs interleaved with double slabs of bromine atoms), as well as its special {001} facets that are terminated with oxygen atoms of high density and thus inclined to generate OVs under very mild conditions (Supporting Information Figure S1).

RESULTS AND DISCUSSION

Theoretical calculation was first used to check the possible N_2 activation on the OVs of BiOBr {001} facets. The chemisorption of N_2 on the hydrogen-stabilized (001) surface of BiOBr was ruled out because of their weak interaction. After generating an OV on the surface, Bader charge of the two OV-connected Bi atoms (Bi_1, Bi_2) in the sublayer increased from 2.87 e to 3.34 and 3.32 e, respectively (Figure 1a,b). This indicated the partial reduction of Bi ions by the localized electrons. Interestingly, N_2 could be adsorbed on the OV through coordinating with the two OV-connected and partially reduced Bi atoms with an end-on bound structure (Figure 1c). Charge density difference was then employed to trace the electrons transfer behavior, which revealed that both the exchange and transfer of electrons mainly took place between the OV and N_2. Obviously, back transfer of charges from OVs

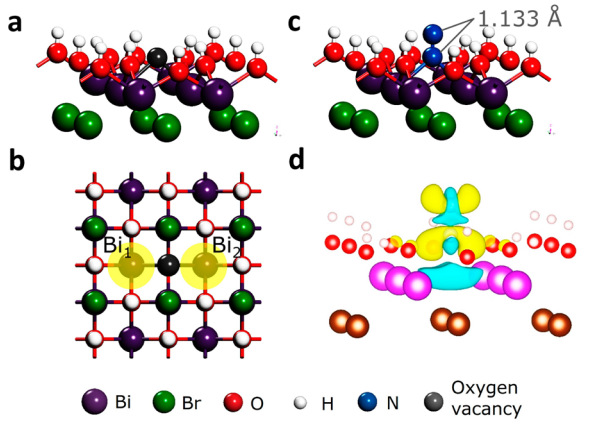

Figure 1. Theoretical prediction of N_2 activation on the OV of BiOBr (001) surface. (a) Side and (b) top view of (001) surface of BiOBr with an OV. (c) The adsorption geometry of N_2 on the OV of BiOBr (001) surface. (d) The charge density difference of the N_2-adsorbed (001) surface. The yellow and blue isosurfaces represent charge accumulation and depletion in the space, respectively. For clarity, the symmetric parts of the optimized slabs at the bottom are not shown. The isovalue is 0.002 au.

to the adsorbed N_2 (as depicted by the electron depletion on the OV and electron accumulation on the adsorbed N_2) suggests the possible N−N triple bond activation. Such interesting electron back-donation phenomenon can be found in many transition metal−N_2 complexes, in which the transitional metals (metal = Fe, Mo, Ru and Co) donate their available d-orbital electrons into the π N−N antibonding system to activate the $-N_2$ ligand.[22−24] The coordinated and activated N_2 create molecular steps mediating the formation of high-energy intermediates ($-N_2^-$, $-N_2H$ or —HN═NH) en route to the final product of NH_3 or N_2H_4 via successive proton and electron transfer.[25,26] The extent of N−N triple bond activation (weakening) over the OV in our case can be reflected by the N−N bond length increased to 1.133 Å, which is between the triple bond length (1.078 Å) of free molecular nitrogen and the double bond length (1.201 Å) of diazene.

Inspired by the theoretical calculation results, we adopted a simple solvothermal method to synthesize {001} facet exposed BiOBr nanosheets of OVs (BOB-001-OV) (Supporting Information Figure S2).[27] A reference photocatalyst without OVs (BOB-001-H) can be obtained by annealing BOB-001-OV in the saturated O_2 atmosphere at 300 °C (Supporting Information Figure S3). Using water as the solvent and proton source, we subsequently evaluated the photocatalytic performance of BiOBr nanosheets of OVs under visible light (λ > 420 nm) by spectrophotometrically measuring the generated NH_3 with Nessler's reagent (Figure 2a). No significant amount of NH_3 was detected in the case of BOB-001-H photocatalysis with or without N_2 after 60 min, while BOB-001-OV could generate a significant amount of NH_3 in the atmosphere of N_2 and the concentration of NH_3 increased linearly along with time (Figure 2b). The visible light driven photocatalytic N_2 fixation rate was estimated to be 104.2 μmol/h per one gram of catalyst of BOB-001-OV. To the best of our knowledge, this is the first report on the visible light driven N_2 fixation without using any organic scavengers or precious-metal cocatalysts. Under UV−vis light, the photocatalytic N_2 fixation rate over BOB-001-OV increased to 223.3 μmol/h per one gram of catalyst (Supporting Information Figure S4a). Control experi-

DOI: 10.1021/jacs.5b03105
J. Am. Chem. Soc. 2015, 137, 6393−6399

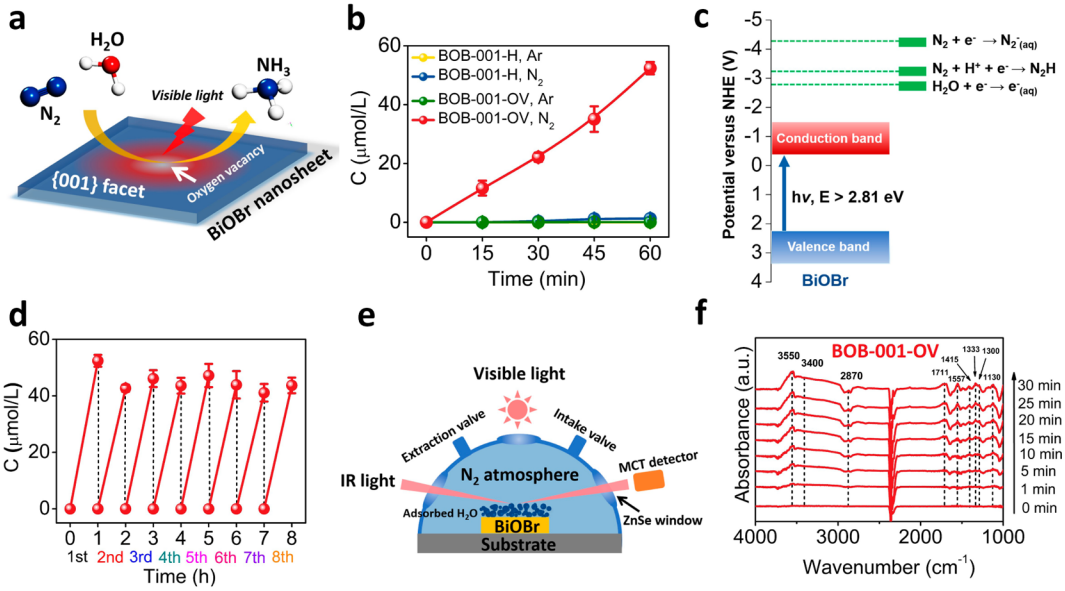

Figure 2. Photocatalytic N_2 fixation over the as-prepared BiOBr nanosheets. (a) Schematic illustration of the photocatalytic N_2 fixation model in which water serves as both the solvent and proton source. (b) Quantitative determination of the generated NH_3 under visible light ($\lambda > 420$ nm). (c) Electronic energy-level diagram of BOB-001-OV. (d) Multicycle N_2 fixation with BOB-001-OV. (e) Designed reaction cell for the in situ IR signal recording. A layer of water molecules, which were necessary to provide protons in our functional model, was first preadsorbed on the surface through bubbling a small amount of water vapor before the large amount of N_2 was pumped in to construct a saturated N_2 atmosphere. At last, visible light was turned on and the IR signal was in situ collected through a MCT detector along with the reaction. (f) In situ FTIR spectra recorded during the photocatalytic N_2 fixation over BOB-001-OV. The error bars arise from values extracted from several measurements on multiple catalysts.

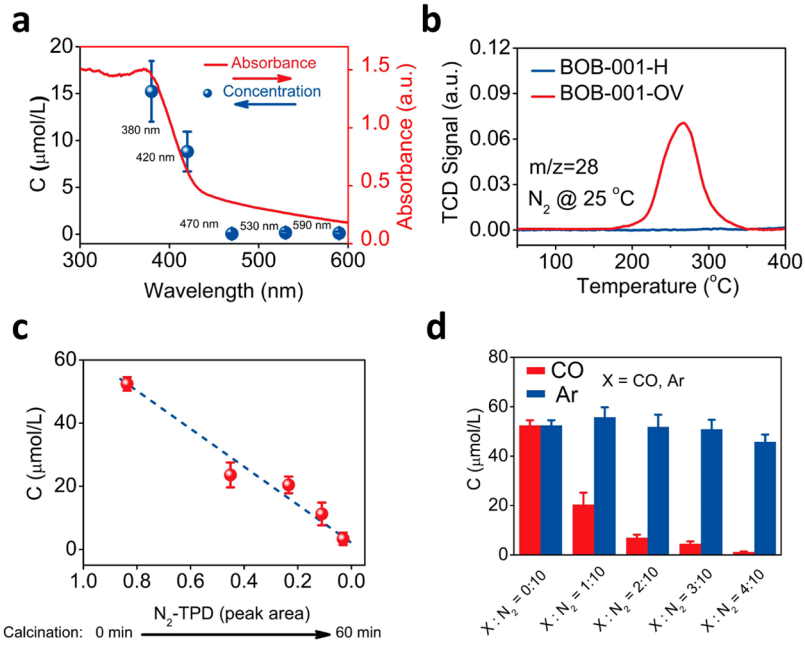

Figure 3. Influence of monochromatic light wavelength, OVs' amount, and CO on the photocatalytic N_2 fixation over BOB-001-OV. (a) N_2 fixation by BOB-001-OV under monochromatic light along with its light absorption spectra. (b) N_2-TPD profiles of the as-prepared BiOBr photocatalysts. (c) N_2 fixation performance of the calcined BOB-001-OV as a function of the corresponding area of N_2-TPD peak. (d) Effect of CO on the photocatalytic fixation of N_2 over BOB-001-OV. (The Ar/N_2 mixture gas was used for comparison.) The error bars arise from values extracted from several measurements on multiple catalysts.

ments with using aprotic solvents (CH_3CN and DMF) instead of water revealed nongeneration of NH_3, confirming the necessity of H_2O as the proton source for the photocatalytic N_2 fixation (Supporting Information Figure S4b). The addition of the electron scavenger $AgNO_3$ significantly suppressed the N_2 fixation photoreactivity of BOB-001-OV (Supporting Information Figure S4c), indicating the primary active species were the photoexcited electrons.

Similar with other traditional semiconductors, conduction band (CB) potential of BiOBr was incapable of directly reducing N_2 or forming solvated electrons (Figure 2c),[28] suggesting the activation of N_2 adsorbed on the BiOBr surface

DOI: 10.1021/jacs.5b03105
J. Am. Chem. Soc. 2015, 137, 6393−6399

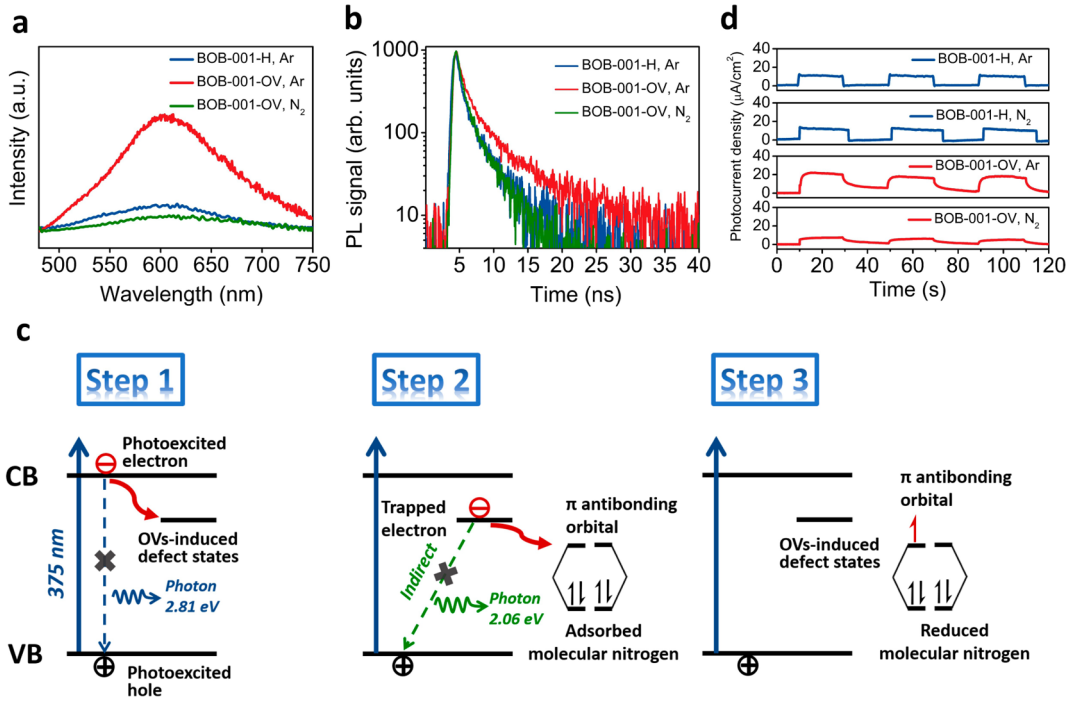

Figure 4. Characterization and discussion the possible charge carriers' dynamics. The Ar and N_2 atmosphere respectively simulates the inert and reactive environment. (a) Room-temperature steady-state PL spectra of the as-prepared BiOBr photocatalysts. (b) The corresponding decay curves. (c) Schematic illustration for enhanced interfacial electron transfer processes induced by OVs. OVs-induced defect states first dynamically trap the directly excited electrons from the CB of BiOBr, thus suppressing the direct recombination of charge carriers (Step 1 and 2). Subsequently, the indirect recombination of trapped electrons with photoexcited holes is also suppressed as the trapped electrons could efficiently be transferred to populate the empty antibonding orbitals of adsorbed N_2 (Step 3). (d) Transient photocurrent responses of different BiOBr photocatalysts.

of OVs as revealed by the theoretical calculation results. After 8 times of cycling test, no significant photoreactivity decrease was observed, indicating the photostability of BOB-001-OV for the visible light N_2 fixation (Figure 2d). To directly visualize the N_2 reduction on the OVs of {001} facets, we employed in situ diffuse reflectance Fourier transform infrared (FTIR) spectroscopy to monitor the time-dependent change of the functional groups on the BiOBr surface under visible light in a designed reaction cell (Figure 2e). No significant change was observed on the FTIR spectra of BOB-001-H (Supporting Information Figure S4). As for BOB-001-OV, several absorption bands gradually increased with the irradiation time for 0 to 30 min in the N_2 atmosphere (Figure 2f). A predominant overlapped absorption band ranging from 3000 to 3700 cm^{-1} was first observed, where the sharp band at 3550 cm^{-1} and the broad band at 3400 cm^{-1} were assigned to the ν(N−H) stretching mode and the ν(O−H) stretching mode of surface hydroxyl groups or adsorbed water, respectively. Besides, the two absorption bands at 1711 and 1557 cm^{-1} could be attributed to the σ(N−H) bending mode, while the band at 1333 cm^{-1} was assigned to the σ(O−H) bending mode. Moreover, the bands at 1300 and 1190 cm^{-1} were ascribed to the molecularly adsorbed NH_3 and the weak absorption bands at 2870 and 1415 cm^{-1} were arisen from the characteristic absorption of NH_4^+. These results strongly revealed that the introduction of OVs on the surface significantly enhanced the visible light N_2 fixation efficiency of BiOBr.

The electron-donating nature of excited BOB-001-OV for photocatalytic N_2 reduction was first proved by no trace of NH_3 detected during N_2 fixation over BOB-001-OV in the dark (Supporting Information Figure S5). Meanwhile, the trend of N_2 fixation of BOB-001-OV just matched with its absorption spectra under the monochromatic light of 380 and 420 nm, which could directly excite BiOBr (Figure 3a). However, the monochromatic light of wavelength (470, 530, and 590 nm) longer than the absorption edge (440 nm) of BiOBr could not induce the N_2 reduction, although these monochromatic lights might indirectly excite BOB-001-OV of distinct absorption tail in the whole visible light region. These results suggested that the number of localized electrons on the OVs were insufficient to complete the complicated six-electron reduction of N_2 adsorbed on the OVs of BiOBr {001} facets through the indirect sub-bands excitation, but direct excitation of BiOBr did work.

As the OVs of BiOBr nanosheets are regarded as the catalytic centers capable of adsorbing and activating N_2, the N_2 reduction efficiency over BOB-001-OV would be highly dependent on the presence of OVs. To verify this point of view, temperature-programmed desorption of N_2 (N_2-TPD) was first employed to investigate the N_2 adsorption on the OVs. A single desorption peak of N_2 began to appear at 176 °C and centered at 265 °C for BOB-001-OV, which is related to chemisorbed N_2, but no adsorption of N_2 was observed on BOB-001-H (Figure 3b). This difference confirmed the indispensable role of OVs on the N_2 adsorption. Subsequently, we calcined BOB-001-OV in the saturated O_2 atmosphere at 300 °C for different time to obtain BiOBr nanosheets with decreased amount of OVs on the {001} facets (Supporting Information Figure S6). As expected, the NH_3 yields of different BOB-001-OV samples were linearly related to the peak area of their N_2-TPD peak (Figure 3c), suggesting both the adsorption and the reduction capacity of N_2 of BOB-001-OV were highly dependent on the OVs amount. Moreover, after the interfacial charge transfer from BiOBr to N_2 was

DOI: 10.1021/jacs.5b03105
J. Am. Chem. Soc. 2015, 137, 6393−6399

blocked by coating an insulator layer of SiO_2 on BOB-001-OV surface,[29,30] the generation of NH_3 was significantly suppressed (Supporting Information Figure S7). We also interestingly found that BOB-001-OV exhibited nitrogenase-like CO-inhibiting phenomenon.[31] For instance, bubbling a mixture gas of CO/N_2 ranging from 1:10 to 4:10 gradually inhibited the generation of NH_3 (Figure 3d), which was not observed in the case of Ar/N_2 mixture gas. This difference can be attributed to the difficult reducibility of CO and its stronger adsorption on the OVs than N_2.[32]

As aforementioned, the OVs-induced defect states might act as the initial charge carriers acceptor to inhibit electron/hole recombination, and also promote the interfacial charge transfer from the excited BiOBr nanosheets to preactivated N_2 on the OVs. To confirm this hypothesis, room-temperature steady-state and time-resolved photoluminescence (PL) spectroscopy were employed to get collective information on the influences of OVs and N_2 on the charge carrier dynamics (separation, trap, transfer and recombination). Under the Ar atmosphere, BOB-001-OV possessed a broader and more intense peak centered at about 600 nm in the steady-state PL, compared with BOB-001-H (Figure 4a). This PL emission of lower energy emission transition was arisen from the indirect radiative recombination of electrons trapped at OVs-induced defect states (located about 0.47 eV below the CB edge) with the holes at valence band (VB). The PL peak decay of BOB-001-OV was much slower than that of BOB-001-H (Figure 4b), which were fitted most reasonably by a double-exponential model using eq 1, where $I(t)$ is the intensity of PL signal, τ_1 and τ_2 are the decay times, and A_1 and A_2 are the corresponding magnitudes. The double-exponential model suggested that two emissive states were involved in the PL decay with τ_1 = 0.37 ns and τ_2 = 3.01 ns. The fast decay component (τ_1) was attributed to the radiative emission of direct interband exciton recombination, and the much slower component (τ_2) was originated from the radiative emission via indirect recombination of trapped electrons with VB holes.[33−35] Direct recombination of excitons was predominated in BOB-001-H, as revealed by its higher proportion of short-living component ($A_1\tau_1$, 74.2%). More efficient trapping of electrons on the OVs states of BOB-001-OV resulted in a higher proportion of long-living defect level component ($A_2\tau_2$, 67.4%) (Supporting Information Table S1). The corresponding average lifetime ($\tau_{BOB\text{-}001\text{-}OV}$ = 2.15 ns) of the PL spectra of BOB-001-OV was over two times longer that of BOB-001-H ($\tau_{BOB\text{-}001\text{-}OV}$ = 1.06 ns), revealing that OVs-induced trapping sites as the initial electron acceptor significantly increased the lifetime of charge carriers. When the Ar atmosphere was replaced with the N_2 atmosphere, the steady-state PL spectra of BOB-001-OV was significantly quenched, accompanying with a reduced PL efficiency. The quenched PL decay spectra of BOB-001-OV under the N_2 atmosphere was found to almost coincide with that of BOB-001-H under the Ar atmosphere, along with the proportion of indirect excitons' recombination largely decreased from 67.4 to 36.8%. Typically, the efficiency of a PL emission (η) is determined both by radiative recombination and nonradiative quenching processes, as given by eq 2, where I_r and I_{nr} are respectively the radiative and nonradiative transition probabilities.[36] Thus, the PL emission efficiency/intensity can be enhanced by radiative recombination and reduced by non-radiative quenching of charge carriers. As the electrons trapped on the OVs are usually in the metastable state, the quenching of PL spectra of BOB-001-OV under the N_2 atmosphere is possibly attributed to nonradiative transfer of trapped electrons to the π antibonding orbitals of adsorbed N_2 (Figure 4c). As expected, the SiO_2 coated BOB-001-OV, which blocked the interfacial electron transfer, exhibited no significant change of the (steady-state or time-resolved) PL spectra under the Ar and N_2 atmosphere (not shown here). This indirectly reflected the OVs as the initial electron acceptor significantly promoted the interfacial electron transfer. Transient photocurrent responses of the as-prepared BiOBr nanosheets further confirmed this point of view. There was no difference between the transient photocurrent responses of BOB-001-H under the Ar and N_2 atmosphere, indicating the interfacial electron transfer of BOB-001-H was not disturbed by the surrounding N_2. Intriguingly, the photocurrent density of BOB-001-OV under the N_2 atmosphere was merely 1/3 of that under the Ar atmosphere, indicative of the strong interaction between the surface OVs with N_2 (Figure 4d). Assuming that the excitation of BOB-001-H and BOB-001-OV are of equal probability under the same light source, the presence of OVs was highly favorable for the interfacial electron transfer from the excited BiOBr nanosheets to the adsorbed N_2. The rate of electrons being transferred from trapped states of OVs to the adsorbed N_2 was roughly estimated to be 3.2×10^8 s^{-1}, as calculated by $(N_2\text{-}\tau_{BOB\text{-}001\text{-}OV})^{-1} - (Ar\text{-}\tau_{BOB\text{-}001\text{-}OV})^{-1}$, where $N_2\text{-}\tau_{BOB\text{-}001\text{-}OV}$ and $Ar\text{-}\tau_{BOB\text{-}001\text{-}OV}$ are respectively the PL spectra average lifetimes of BOB-001-OV under the N_2 and Ar atmosphere.[37] Thus, the interfacial electron transfer rate of BOB-001-OV was nearly 5 orders of magnitude faster than that (5.2×10^3 s^{-1}) of BOB-001-H under the N_2 atmosphere.

$$I(t) = A_1\exp(-t/\tau_1) + A_2(-t/\tau_1) \quad (1)$$

$$\eta = I_r/(I_r + I_{nr}) \quad (2)$$

Usually, photocatalytic N_2 fixation to NH_3 is of poor selectivity with generating considerable amount of byproducts such as N_2H_4, NO_2^- and NO_3^-.[38−40] In this study, the amounts of these byproducts were tiny (2.4% for N_2H_4, and 1.9% for NO_3^-), possibly because of the end-on coordinating mode of N_2 and the negligible NH_3 oxidation by the in situ formed O_2 (Supporting Information Figure S8a,b,c). The amount of in situ formed O_2 was close to 3/4 of the generated NH_3 amount in the early stage in a sealed reactor (Supporting Information Figure S8d), revealing that water could efficiently act as the sacrificial electron donor of photogenerated holes. Therefore, the overall reaction of N_2 reduction in this study could be described with eq 3. However, the effect of in situ formed O_2 on the OVs of BiOBr cannot be ignored. The OVs would be quenched to decrease the photoreactivity if the in situ formed O_2 was not removed from the reaction medium in time (Supporting Information Figure S8e).[27] Fortunately, most of the in situ formed O_2 could be swept off from the aqueous solution in an open reactor under the continuous N_2 purging, which could avoid the undesirable oxidation of NH_3 and also maintain the stability of OVs.[41]

$$2N_{2(g)} + 6H_2O_{(1)} \rightarrow 4NH_{3(g)} + 3O_{2(g)} \quad (\text{BiOBr of OVs}, \lambda > 420\text{nm}) \quad (3)$$

CONCLUSIONS

In summary, we demonstrate that atmospheric N_2 can be efficiently reduced to NH_3 by BiOBr nanosheets of OVs under visible light, without using any organic scavengers and precious-

DOI: 10.1021/jacs.5b03105
J. Am. Chem. Soc. 2015, 137, 6393−6399

metal cocatalysts. Along with the electron-donating nature of BiOBr under visible light, the designed catalytic centers of OVs could activate N_2 and significantly promote the interfacial electron transfer from the excited BiOBr nanosheets to the adsorbed N_2 (Supporting Information Figure S9). The N_2 fixation rate of BOB-001-OV in this study was much higher than those of other semiconductors (Supporting Information Table S2). Actually, the external quantum efficiency of this prototype N_2 fixation at 420 nm monochromatic light has reached 0.23% within 60 min for this complicated six-electron reduction process. Although photocatalytic reduction is unlikely to replace the Haber–Bosch process at present, this study might open up a new vista to fix atmospheric N_2 to NH_3 through less energy-demanding photochemical process.

EXPERIMENTAL SECTION

Chemicals. All chemicals used were purchased from Sinopharm Chemical Reagent Co., Ltd. (Shanghai, China) and were of analytical grade and used without purification.

Preparation of {001} Facets Exposed BiOBr of OVs. For the preparation of BiOBr microsphere assembled by {001} facets exposed single crystalline nanosheets, 1.5 mmol $Bi(NO_3)\cdot 5H_2O$ were added slowly into 16 mL of ethylene glycol solution containing stoichiometric amounts of KBr. The mixture was stirred for 1 h at room temperature in air, and then poured into a 20 mL Teflon-lined stainless autoclave. The autoclave was allowed to be heated at 160 °C for 12 h under autogenous pressure, and then air cooled to room temperature. The resulting precipitates were collected and washed with deionized water and ethanol to remove the residual ions. The final product was dried at 60 °C in air for further use. The corresponding sample was designated as BOB-001-OV. For comparison, the counterpart sample without OVs on the {001} facets was synthesized by heating BOB-001-OV at 300 °C in the saturated O_2 atmosphere for 4 h to reoxidize the surface and was denoted as BOB-001-H.

DFT Theoretical Calculation. All calculations were performed using the first-principles density of functional theory (DFT) + U calculations with the exchange-correlation energy functional, which were described by generalized gradient approximation with the by Perdew–Burke–Ernzerhof (PBE) exchange-correlation function.[42] The calculations were performed using the Vienna Ab-initio Simulation Package (VASP) with a plane-wave cutoff energy of 520 eV.[43,44] To simulate the molecular nitrogen activation on surfaces, a (2 × 2) supercell with the vacuum thickness being larger than 20 Å was used. During optimizations, the energy and force converged to 10^{-5} eV/atom and 0.02 eV/Å, respectively. The k-points were 3 × 3 × 1 for optimizations and increased to 7 × 7 × 1 for the band energy and DOS calculations of the BOB-001 structure.

Photocatalytic Activity Test. All photocatalytic activity experiments were conducted at ambient temperature using a 300 W xenon lamp with a 420 nm cutoff filter to simulate visible light, respectively. For the fixation of molecular nitrogen, 0.05 g of photocatalyst was added into 100 mL of double distilled water in a reactor. The reactor was equipped with water circulation in the outer jacket in order to maintain at room temperature of 25 °C. The mixture was continuously stirred in the dark and under visible light with high-purity N_2 bubbled at a flow rate of 60 mL/min for 30 and 60 min, respectively. Five milliliters of the solution was taken out each 15 min and after centrifuged to remove the photocatalyst, and the concentration was monitored by colorimetry with the Shimadzu UV-2550 UV–vis spectrometer. Five LED light (UVEC-4II, Shenzhen Lamplic Technology Co. Ltd. China) with total light intensity of 10 W/cm^2 was utilized as a monochromatic light source. The external quantum efficiency at 420 nm was calculated on the basis of the following equation: external quantum efficiency = 100% × (number of generated ammonia × 6)/number of incident photons. Oxidation of water was carried out in a Pyrex reaction cell under 300 W xenon lamp with a 420 nm cutoff filter, which was sealed with a glass stopper and connected to a N_2 balloon. At certain time intervals, liquid (NH_3) and gas (O_2) composition were respectively determined by the Nessler's reagent and gas chromatography (Trace 1300-ISQ, Thermo).

ASSOCIATED CONTENT

Supporting Information

Other experimental details, additional SEM and TEM images, X-ray diffraction patterns (XRD), UV–vis diffuse reflectance spectra (DRS), and additional data as well as the possible mechanism. This material is available free of charge via the Internet at http://pubs.acs.org.

AUTHOR INFORMATION

Corresponding Author

*zhanglz@mail.ccnu.edu.cn

Notes

The authors declare no competing financial interest.

ACKNOWLEDGMENTS

This work was supported by National Natural Science Funds for Distinguished Young Scholars (Grant 21425728), National Basic Research Program of China (973 Program) (Grant 2013CB632402), National Science Foundation of China (Grants 21177048, and 51472100), and Key Project of Natural Science Foundation of Hubei Province (Grant 2013CFA114).

REFERENCES

(1) Chase, M. W. *NIST-JANAF Thermochemical Tables*, 4th ed; American Chemical Society and American Institute of Physics Press: New York, 1998.
(2) Rafiqul, I.; Weber, C.; Lehmann, B.; Voss, A. *Energy* **2005**, *30*, 2487.
(3) Ritter, S. K. *Chem. Eng. News* **2008**, *86*, 53.
(4) Smil, V. *Enriching the Earth: Fritz Haber, Carl Bosch, and the Transformation of World Food Production*; MIT Press: Cambridge, MA, 2004.
(5) Canfield, D. E.; Glazer, A. N.; Falkowski, P. G. *Science* **2010**, *330*, 192.
(6) Shah, V. K.; Brill, W. J. *Proc. Natl. Acad. Sci. U. S. A.* **1977**, *74*, 3249.
(7) Kim, J.; Rees, D. *Biochemistry* **1994**, *33*, 389.
(8) Dean, D. R.; Bolin, J. T.; Zheng, L. *J. Bacteriol.* **1993**, *175*, 6737.
(9) Lee, S. C.; Holm, R. H. *Chem. Rev.* **2004**, *104*, 1135.
(10) Schrauzer, G. N.; Guth, T. D. *J. Am. Chem. Soc.* **1977**, *99*, 7189.
(11) Liang, Y. T.; Vijayan, B. K.; Gray, K. A.; Hersam, M. C. *Nano Lett.* **2011**, *11*, 2865.
(12) Walter, M. G.; Warren, E. L.; McKone, J. R.; Boettcher, S. W.; Mi, Q.; Santori, E. a; Lewis, N. S. *Chem. Rev.* **2010**, *110*, 6446.
(13) Britto, P. J.; Santhanam, K. S. V.; Rubio, A.; Alonso, J. a.; Ajayan, P. M. *Adv. Mater.* **1999**, *11*, 154.
(14) Zhu, D.; Zhang, L.; Ruther, R. E.; Hamers, R. J. *Nat. Mater.* **2013**, *12*, 836.
(15) Tan, S.; Ji, Y.; Zhao, Y.; Zhao, A.; Wang, B.; Yang, J.; Hou, J. G. *J. Am. Chem. Soc.* **2011**, *133*, 2002.
(16) Aschauer, U.; Chen, J.; Selloni, A. *Phys. Chem. Chem. Phys.* **2010**, *12*, 12956.
(17) Lee, J.; Sorescu, D. C.; Deng, X. *J. Am. Chem. Soc.* **2011**, *133*, 10066.
(18) Liu, L.; Zhao, C.; Li, Y. *J. Phys. Chem. C* **2012**, *116*, 7904.
(19) Tian, N.; Zhou, Z.-Y.; Sun, S.-G.; Ding, Y.; Wang, Z. L. *Science* **2007**, *316*, 732.
(20) Green, I. X.; Tang, W.; Neurock, M.; Yates, J. T. *Acc. Chem. Res.* **2014**, *47*, 805.
(21) Christopher, P.; Xin, H.; Linic, S. *Nat. Chem.* **2011**, *3*, 467.
(22) Tanabe, Y.; Nishibayashi, Y. *Coord. Chem. Rev.* **2013**, *257*, 2551.
(23) Jia, H.-P.; Quadrelli, E. A. *Chem. Soc. Rev.* **2014**, *43*, 547.

DOI: 10.1021/jacs.5b03105
J. Am. Chem. Soc. 2015, 137, 6393–6399

(24) Sivasankar, C.; Baskaran, S.; Tamizmani, M.; Ramakrishna, K. *J. Organomet. Chem.* **2014**, *752*, 44.
(25) Leigh, G. J. *Acc. Chem. Res.* **1992**, *25*, 177.
(26) Schrock, R. R. *Acc. Chem. Res.* **2005**, *38*, 955.
(27) (a) Li, H.; Shi, J.; Zhao, K.; Zhang, L. *Nanoscale* **2014**, *6*, 14168. (b) Li, J.; Yu, Y.; Zhang, L. *Nanoscale* **2014**, *6*, 8473. (c) Jiang, J.; Zhang, L. Z.; Li, H.; He, W. W.; Yin, J. J. *Nanoscale* **2013**, *5*, 10573.
(28) Fang, Y.-F.; Ma, W.-H.; Huang, Y.-P.; Cheng, G.-W. *Chem.—Eur. J.* **2013**, *19*, 3224.
(29) Awazu, K.; Fujimaki, M.; Rockstuhl, C.; Tominaga, J.; Murakami, H.; Ohki, Y.; Yoshida, N.; Watanabe, T. *J. Am. Chem. Soc.* **2008**, *130*, 1676.
(30) Takahashi, T.; Kudo, A.; Kuwabata, S.; Ishikawa, A.; Ishihara, H.; Tsuboi, Y.; Torimoto, T. *J. Phys. Chem. C* **2013**, *117*, 2511.
(31) Rivera-Ortiz, J. M.; Burris, R. H. *J. Bacteriol.* **1975**, *123*, 537.
(32) Rusina, O.; Linnik, O.; Eremenko, A.; Kisch, H. *Chem.—Eur. J.* **2003**, *9*, 561.
(33) Han, N. S.; Shim, H. S.; Seo, J. H.; Kim, S. Y.; Park, S. M.; Song, J. K. *J. Appl. Phys.* **2010**, *107*, 084306.
(34) Iijima, K.; Goto, M.; Enomoto, S.; Kunugita, H.; Ema, K.; Tsukamoto, M.; Ichikawa, N.; Sakama, H. *J. Lumin.* **2008**, *128*, 911.
(35) Dozzi, M. V.; D'Andrea, C.; Ohtani, B.; Valentini, G.; Selli, E. *J. Phys. Chem. C* **2013**, *117*, 25586.
(36) Wang, Y. G.; Lau, S. P.; Lee, H. W.; Yu, S. F.; Tay, B. K.; Zhang, X. H.; Hng, H. H. *J. Appl. Phys.* **2003**, *94*, 354.
(37) Bian, Z.; Tachikawa, T.; Zhang, P.; Fujitsuka, M.; Majima, T. *Nat. Commun.* **2014**, *5*, 3038.
(38) Linnik, O.; Kisch, H. *Photochem. Photobiol. Sci.* **2006**, *5*, 938.
(39) Ileperuma, O. A.; Weerasinghe, F. N. S.; Lewke Bandara, T. S. *Sol. Energy Mater.* **1989**, *19*, 409.
(40) Zhao, W.; Zhang, J.; Zhu, X.; Zhang, M.; Tang, J.; Tan, M.; Wang, Y. *Appl. Catal., B* **2014**, *144*, 468.
(41) Tennakone, K.; Wickramanayake, S.; Fernando, C. A. N.; Ileperuma, O. A.; Punchihewa, S. *J. Chem. Soc. Chem. Commun.* **1987**, *14*, 1078.
(42) Kresse, G. *Phys. Rev. B: Condens. Matter Mater. Phys.* **1996**, *54*, 11169.
(43) Perdew, J. P.; Burke, K.; Ernzerhof, M. *Phys. Rev. Lett.* **1996**, *77*, 3865.
(44) Kresse, G. *Phys. Rev. B: Condens. Matter Mater. Phys.* **1999**, *59*, 1758.

DOI: 10.1021/jacs.5b03105
J. Am. Chem. Soc. 2015, 137, 6393−6399